IIETA International Information and Engineering Technology Association
Advancing the World of Information and Engineering

Traitement du Signal
Vol. 39, No. 1, February, 2022, pp. 31-42
Journal homepage: http://iieta.org/journals/ts

Heart Disease Detection Based on Feature Fusion Technique with Augmented Classification Using Deep Learning Technology

Kayam Saikumar[1*], Vullanki Rajesh[1], Bulepe Sankara Babu[2]

[1] Departments of ECE, Koneru Lakshmaiah Education Foundation, Guntur 522502, India
[2] Dept. of CSE, Gokaraju Rangaraju Institute of Engineering and Technology (Autonomous), Bachupally, Hyderabad 500090, Telangana, India

Corresponding Author Email: rajesh4444@kluniversity.in

https://doi.org/10.18280/ts.390104

Received: 31 December 2021
Accepted: 12 February 2022

Keywords:
heart disease, classification, deep learning, feature fusion, feature extraction, dimensionality reduction, ALEXNET CNN, RRS segmentation

ABSTRACT

An accurate prediction of cardiac disease is a crucial task for medical and research organizations. Cardiac patients are usually facing heart attacks sometimes tends to death. Therefore, a prior stage of heart diagnosis is compulsory, so that model of optimal Deep learning technology is prosperous for the healthcare sector. The earlier models related to this research work are outdated, some applications cannot provide efficient outcomes. The available conventional models like the Genetic algorithm (GA), PSO (particle swarm optimization), RFO (Random Forest optimization), X-boosting. KNN and many available technologies are only dispensing abnormality information but they are not providing location, depth, and affected area dimensions. Moreover, earlier models only supported fixed scanning in radiology not supporting cloud-level deployment. The sensitivity and robustness of diagnosis are very low therefore a DCAlexNet CNN deep learning technology is needed. The deep learning-based classification is performed through the DCAlexNet CNN (convolutional Neural networks) technique. The implementing application is loading training samples from Kaggle or ANDI dataset. The uploaded image samples are pre-processed through resolution, intensity, and brightness adjustment in the python NumPy tool. The. CSV file (text file) is processed through clustering as well as dimensionality adjusting technique. The processed images are segmented through RRF (Restrictive Random Field) technology. The segmentation on images provides features that are loaded in the local server after that saved into CNN memory. Now the .csv file and trained features are applied to DCAlexNet CNN deep learning architecture. The training processing can give information about diseases in the heart and dimensionality of the affected area (depth and location). Now the application is waiting for real-time samples which is nothing but testing, in this testing part locally available affected and healthy heart ultrasound images are given to DCAlexNet CNN. The designed application can easily be identified whether the uploaded image has abnormality or not. The test-based and image-oriented feature fusion can help the application detect heart abnormalities in an easy way. To this feature fusion-based DCAlexNet CNN confusion matrix generates performance measures like accuracy 98.67%, sensitivity 97.45%, Recall 99.34%, and F1 Score 99.34%, these numerical comparison results compete with present technology and outperformance application robustness.

1. INTRODUCTION

In contemporary days, cardiac disease is a common abnormality that causes the death of several persons, and similarly many countries facing heart diagnosis issues. The heart is the supreme necessary organ of the body and its work guarantees the life of an individual. An increasing number of people are suffering from cardiovascular disease (CVD), which includes excessive blood pressure, coronary heart disease, cardiovascular disease, rheumatic heart disease, and stroke. Detection approaches for CVD include cardiac ultrasonography, CV angiography, and cardiovascular magnetic resonance imaging (CVMR). Computed tomography (CT) and resonance Furthermore, the use of CV medical imaging has become an essential diagnostic tool. Therapy for cardiovascular disease (CVD) is becoming more significant. Classification, detection, and segmentation are the most frequently used tasks in CV medical image analysis nowadays. For CV medical imaging, the big data era has arrived as to how to extract relevant information from a vast number of CV medical pictures and deliver more accurate clinical diagnostics. Coronary abnormality determines heart work [1] and induces a patient's health issues causes death. One of the important issues of cardiac disease is examining a patient's chances for the lack of sufficient bloodstream to the heart. The application of several longitudinal examinations of self-sufficient degeneration and investigation may build the expectation of technique. The massive quantity of data set information should be stored via mechanical progression in the medical care offices and this is the unusually moving position for the information decryption.

A section of the fundamental attributes is Age, Sex, Cholesterol, FBP (Fasting pulse), rest ECG (Electrocardiogram) [2]. Weight, height, smoking habit, diet,

obesity, serum cholesterol, hypertension, pain location, circulatory strain, ECG (heart electrical action test, ST sadness, Threat circulatory strain, Thalach, and several major fluoroscopic vessels are employed in cardiac disease. The human heart's different segments participate in the aorta, aortic valve, aspiratory course, cava, internal vena cava, left the chamber, mitral valve, pneumonic valve, predominant vena right chamber, right ventricle, and tricuspid valve. Regardless of the case, the computation of selecting and joining various highlights depicts an impressive test.

Alongside recently, certain AI calculations like ANN, K-Nearest Neighbor (KNN), and SVM are employed in the Internet of Things (IoT) positioned frameworks for expectation and order. Independent AI calculations are employed to specify the information that is collected by the unique IoT gadgets shown in above Figure 1. The information that is signified by the AI calculations provides many accurate outcomes when compared to manual naming. Subsequently, Neural network-based devices attain the finest in the execution of class for the anticipation of heart and mind disease. Carotid Artery Stenting (CAS) has been increasingly popular in the medical sector in recent years. In the early stages of HD patients, this CAS approach gives an overview of Major Adverse Cardiovascular Events (MACE). The ANN supplies perfecter outcomes when compared with the primary CAS strategy. The suggested ANN-based strategy does not fairly incorporate back probabilities hitherto, besides, produce vales [check spelling] from various archetype procedures. The ANN-based technique attains much better outcomes when compared with existing strategies [3].

Despite the fact that this is a strong tool, the technology used to diagnose cardiovascular disease (CVD) is not fully explored in this work. AI and DL diagnostics paradigm shifts are discussed, as well as possible solutions to probable problems, and the future of the linked machine intelligence applications are envisioned. The challenges described are broken down into the modular parts of DL in terms of CVD picture categorization, segmentation, and detection. The key to a successful technical application of DL in current medical research is a good viewpoint on management of these challenges.

The remainder of this investigation is structured as follows: The second section displays artwork that is related to the first. Segment 3 portrays substances and techniques for the realization of coronary sickness. Area 4 portrays the activity effects of proposed engineering. Segment 5 concludes the paper.

2. RELATED WORKS

Ventures to ascertain and possibly obstruct unequivocal grown-up content are not a recent one, and there is a captivating work regarding the grown-up content location in the cutting edge. The work in wires 2 DL methods of AlexNet and GoogleNet and accounts that exhibition conceivably expanded by fusing the two organizations for the characterization of the grown-up content. The work in aims at skin locus location for the sifting of the content using the 24 tones changes in normally acquirable recordings and pictures. The article provides substantial evidence that includes key-outlines, key shots, and video groupings. Work in relies on multifaceted inspected positioned investigation displaying the functionality of the proffered technique in the location of the trivial explicit groupings with the discovery rate of 87%. The methodology in engages shading-based skin separating and content compiled with sifting based concerning the identification of skin. Zhang et al. [4] employs the approach of content recovery for content sifting; it is dissected and evaluated using datasets that attain a discovery rate of 93.2%. The authors in showcase a system for site dissections; this system produces a magnified arrangement that is independent of the entrance situations. The authors in combine the methodologies based on key-outline with a MPEG-4 measurable investigation of the stream vectors. The authors in produce sifting toward Web-based P2P. Authors in employ twain visual highlights for accessing the media and separating; the former visual highlight is single casing and latter visual highlight is choice variable of different edges along with Discriminate investigation toward advancement. Picture sifting is originally like substance-based recovery [5].

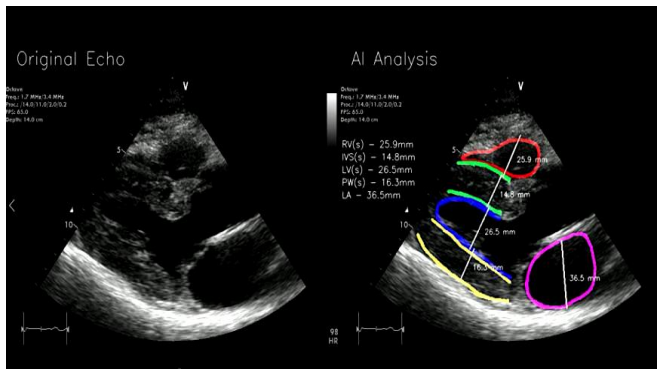

Figure 1. Heart ultrasound image

3. PROPOSED METHODOLOGY

Implemented Design Setup: The Deep learning architecture refers to the learning method of employing to a certain prediction experiment that takes been aimed to estimate the result of the proposed method. Two-category data numerical and image data are assessed separately at first, and when the enhancement of the image is done, the image data is segmented by SIFT later. DCALEXNET CNN and ALEXNET CNN multi-layer perception on the two sets of various data is used to do feature extraction. Then the feature fusion process is used to concatenate the extracted featured trained data. To categorize whether the patient is suffering from severe cardiac disease or not, the Ensemble classifiers like DCALEXNET CNN and ADA Boost. The classifier is implemented to the fusion data. Many performance evaluation metrics are computed to evaluate architecture's performance. All computation experiments have been administered in Python 3.6.5 environment utilizing Deep learning libraries on an Intel® Core™ i3-3217U CPU@1.80 GHz PC. 3.3.

4. PROPOSED SYSTEM MODEL

Suggested Figure 2 shows a deep mastering ensemble architecture employing the ALEXNET CNN and the ALEXNET CNN-Multi-layer perceptron with characteristic fusion. Deep learning algorithms are trained using a data collection generated by Internet of Medical Things (IoMT) legal devices. There are two phases in the proposed

architecture – the pre-processing and the post-processing phases. The pre-processing phase comprises three individual layers that contain the pre-processing, Data enhancement, and Segmentation [6]. This pre-processing obtains raw data, and possibly this could have a few lost values and noise. In this phase, various methods like mean, mode, & average are implied for prognosis of lost values also discard noise employing normalization and eliminate variance data employing dimensionality reduction. Additionally, noise and dimensionality reduction data are received by the Data enhancement in this phase to evaluate the data enhancement so that the pre-processed data has been intensified for further processing shown in below Figure 2. Conversely, in the segmentation, the image data has been segmented to increase the comprehensive training accuracy. In the post-processing phase, the segmented image and the numeric data are directed by the ensemble feature extractor like ALEXNET CNN and ALEXNET CNN Multi-layer perceptron, and the feature data is concatenated by the techniques of feature fusion, and later, the fusion data is managed for the classification.

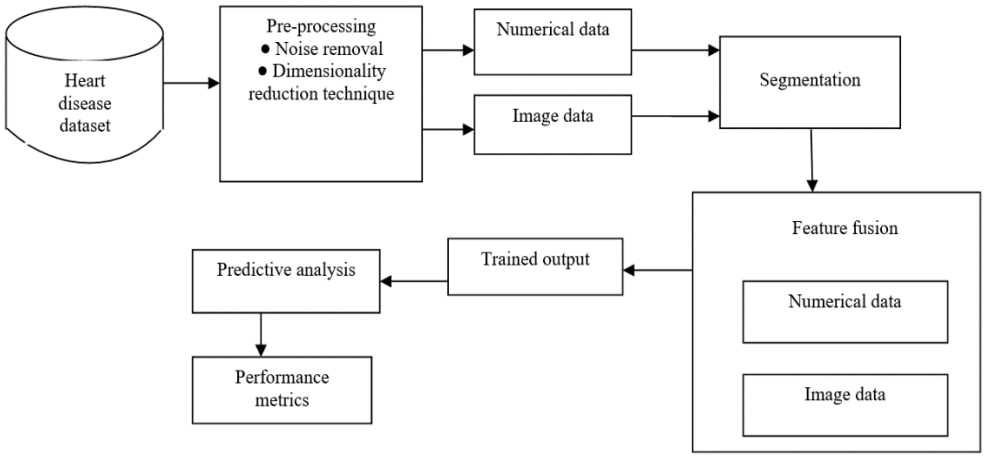

Figure 2. Overall proposed architecture for heart disease using fusion method

The application of Ensemble classifiers like ALEXNET CNN and ADA Boost are used. classifier on the fusion data is used to classify whether the patient is suffering from severe cardiac disease or not. A similar mechanism is implemented in parallel within the proposed architecture [7]. The above Figure 1 is the overall proposed architecture.

4.1 Pre-processing

In above-proposed architecture, pre-processing step included for numerical data like handling moving average, missing values and normalization are explained as follows: Null as well as missing values are entered in data set at the first step since they can direct towards false prediction of any ML method. In this architecture, approach is selected to attribute the out of place or null values when you consider that mean device is splendid because it attributes persistent statistics without introducing outliers. Formulation of mean technique is as follows:

$$Q(y) = \begin{cases} mean(x), & if\ y = \dfrac{null}{missed} \\ y, & otherwise \end{cases} \quad (1)$$

where, y stands for the instances of feature vectors that exist in n-dimensional area, y ∈R established in Eq. (1).

Prior to bestowing every segmentation algorithm, they must be in the identical intensities range. For this intention, the images are pre-processed in two steps namely outlier elimination and scaling [8]. The noise of cine MRI is predominant to the intensities of the pixels, and this factuality is apparent in frames histogram. This factuality results in excessive high-intensity values in histogram diagrams. Thus, the one percent of the outlier intensities is first eliminated and then substituted their intensities with the closest value that is absent in the outlier set of the intensity values. Post to this process, there is however the difference continues owing to the intensity variety prior to normalizing. Hence, the resulting data is scaled into a new range [0,1] that is suitable for the input layer.

4.2 Text data pre-processing

4.2.1 Tokenization

Tokenization is the initial step of Morphological Analysis. The objective of tokenization is to analyze and explore words in sentences. In the commencement, textual data is just a block of characters. The works of the data set are necessary for retrieving information in all the subsequent processes.

4.2.2 Stop-word elimination

The archetypal words present in any text document do not give the meaning of the documents. For instance, articles, pronouns, prepositions fall under this category that is considered as stop-words.

Stemming: Stemming or lemmatization is a method for minimizing the words into their root. In English, several words feasibly are minimized to their base form or stem. For instance, ‘agreed’, ‘agreeing’, ‘disagree’, ‘agreement’, and ‘disagreement’ bestowed on ‘agree’.

4.3 Image data pre-processing

The input dataset has been combined with the dataset for heart disease in this process. For data analysis, IPCA is a comparatively novel computational and statistical methodology. ICA emerged from the community of signal processing in which it was evolved as a vigorous technique for splitting blind sources. For feature transformation, the fundamental ICA model can be written as $s_t = ux_t$, where the

observed feature vectors are represented by xt is n×p matrix, st is n×p matrix is new individual evaluated vectors for classification purposes, u refers to n-n de-mixing matrix that remains employed towards obtain a completely new coordinate method of statistically independent non-Gaussian directions, by major non-Gaussian being initial IC direction. Method functions continuously and initially state most non-Gaussian direction. Using PCA to get whitening lessened xt dimension and thus lessens number of st to be calculated shown in Eq. (2). The amount of chosen PCs in this study is similar to that employed on the PCA. The fixed point-method is executed to assess transformation matrix and independent components succeeding the process of data whitening is completed [9]. Mutual knowledge is named as a measure of dependency amongst random variables. Optimizing their negentropy is similar to decreasing mutual data amongst components. Negentropy in speedy ICA can be greater or much less conveyed as follows:

$$J_G\left(s_{t(i)}\right) \approx \left[E\{G\left(s_{t(i)}\right)\} - E\{G(V)\}\right]^2 \quad (2)$$

wherein G is any non-quadratic feature, V stands a Gaussian variable with unit variance and zero imply, and it's miles a dimensional vector made from certainly one of matrix U.S.A. Rows. As G, numerous capabilities are used. Applying in $s_{t(i)} = u_i^T x_t$ Eq. (3) and Eq. (4), the succeeding optimization problem is obtained:

$$\text{Maximize } J_G\left(s_{t(i)}\right) \approx \left[E\{G\left(s_{t(i)}\right)\} - E\{G(V)\}\right]^2 \quad (3)$$

$$\text{Subject to } E\{(\mu_i^T x)^2\} = 1 \; i = 1,2,\ldots.n \quad (4)$$

4.4 Image enhancement

For every slice in dataset edge map is created. Approach for creation of Edge Map joins 3 individual algorithms: Fast Wavelet Transform, alteration of Spatial Pixel Profile algorithm method and Non-linear diffusion, Figure 1 depicts the Edge Map for a single dataset slice. This method's purpose is to find notable edges in slices that will be utilised for segmentation. Spatial Pixel Profile method operates as below: contemplate a pixel $p \in \mathbb{Z}^2$ in 2-D discrete picture g in value range of pixel gray [0,255]. For the specified pixel position $p = (x_p, y_p)$, a circular area is mentioned at a radius rϵ $\mathbb{N}$ as shown Eq. (5):

$$R_r(p) = \{q\epsilon\, \mathbb{Z}|0 \le \left(x_q - x_p\right)^2 + \left(y_q - y_p\right)^2 \le r^2\} \quad (5)$$

In this condition, the cumulative similarity assessment c(p) of a pixel p is calculation of the whole pixels in circular neighborhood $R_r(p)$ where contrast in grey value of pixel in neighbourhood & grey value of pixel p is smaller than σ, shown in Eq. (6) and Eq. (7).

$$c(p) = \sum_{q\in R_r(p)} b(p,q) \quad (6)$$

$$b(p,q) = \begin{Bmatrix} 1, |g(p) - g(q)| \le \sigma \\ 0, otherwise \end{Bmatrix} \quad (7)$$

Values of c(p) where p is positioned at the image's edge will be lesser than values of c(p) when p is positioned in a homogenous area. Outcome of above-referred to manner remains map c that has extra grayscale values in homogenous regions too lesser greyscale values in areas around edges; by utmost greyscale value, any c(p) can acquire presence variety of pixels in area $R_r(p)$ of radius r:

$$c_{max} = |R_r|$$

If the values of c were standardized to the range [0,1], upturned and then every value of $c(p) > 0.5$ were set to 0.

A lot of varied methods prevail that focus to improve the CT images' local contrast [10]. The majority of them rely on Wavelet bandpass coefficients valves utilizing a nonlinear function. The technique is said wherein the nonlinear function maps the bandpass photographs proven in Figure 3.

This method employs the power-law confined by linear functions minute and huge distinction shown in Figure 3.

$$r(x) = \begin{Bmatrix} G.x.\left(1 - \frac{|x|}{M}\right)^p + x, \; for \; |x| \le M \\ x, \; elsewhere \end{Bmatrix} \quad (8)$$

In a bandpass photograph, the function r(x) represents a mapping in the direction of a brand new fee for the coefficient price x. G denotes a regular benefit thing, M denotes the top restriction of the coefficient's nonlinear enhancement, and p denotes the nonlinear enhancement element said in Eq. (8).

4.5 Image segmentation

Techniques for cardiac segmentation based on FCN can be divided into four categories: (1) Using sophisticated building blocks in networks to supplement network feature learning; (2) diminish the issue of class imbalance by advanced loss functions; (3) Enhance the capacity and robustness of networks by a multi-step, multi-task or multi-view functionality fusion. (4) Propelling the network towards produce further anatomically possible segmenting results through including form priors, adverse losses or geometric restrictions in the preparation to normalize the network [11]. It is also helpful to emphasize that spatial and temporal coherence is used by advanced NNs to improve segmentation accuracy & temporal consistency of segmentation maps in cardiac image segmentation.

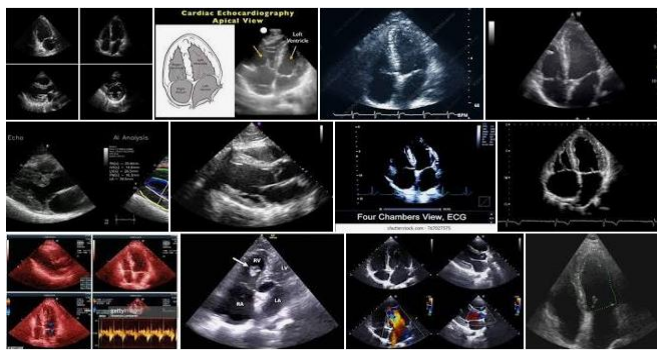

Figure 3. Ultrasound images dataset

5. FEATURE EXTRACTION

Initial function space is transformed right into an extra concise new vicinity inside the feature extraction. In this situation, the specific feature area is converted into concise feature space without removing them however substituting the

former with a minor feature set. That takes region even as the quantity of input statistics' characteristic is widespread to be looked after out, and later the input records may be transformed right into a concise characteristic set of abilities.

5.1 ALEXNET CNN based feature extraction

ALEXNET CNN is employed to automatically create features and merge them with the classifier. Benefits of ALEXNET CNN classifier comprise, out of the whole classifiers, the record of layers that convert input volume to output volume is uncomplicated in this method. There are some unique layers and every layer converts the input to output through a distinguished function. The drawback of this classifier is that it does not encode the position and orientation of the article into their prognoses [12]. A convolution is a considerable leisure operation than, for instance, max pool, both backward and forward. If the network is extensive, every training step is intended to acquire considerably longer.

When the input pictures are transmitted through a succession of layers, such as convolutional, flattening, and fully connected layers pooling, a Convolutional neural network is utilized first, and then a result of ALEXNET CNN is formed to categories video frame images. After establishing ALEXNET CNN models from the scratch, the model is enhanced by using the technique of image augmentation. As a result, one of the pre-trained ALEXNET CNN models is used to categorize images and examine precision for training and validation data.

5.1.1 Pool

This is the pooling layer and is termed as pool. In ALEXNET CNN, max pooling is only used and generally the size of pooling kernel is 2 × 2 along stride of 2.

5.1.2 Fully connected (FC) layer

This layer is executed in ALEXNET CNN along with aid of convolution. Configuration of its size is n1 × n2, where n1 and n2 are the sizes of the input and output tensors accordingly. N1 is a triplet (7 × 7 × 512) whereas n2 is generally an integer.

5.1.3 Dropout

This layer known as "Drop" is utilized for deep learning mechanism enhancement. It locates few of the quantity that has been linked with the particular node percentage network to 0 and MVGG_16 sets it as 0.5 in both the dropout layers.

ReLU layer, which always follow the convolution layer in ALEXNET CNN, boosts the nonlinearity of ALEXNET CNN. The convolution layers present within both the pooling layers possess the equal channel number, kernel size and stride. Actually, collecting two 3×3 convolution layers and three 3 × 3 convolution kernels is equal to a single 5×5 and 7x7 convolution layers respectively. Stacking 2 or 3 small convolution kernels works much quicker than a single huge convolution kernel. Moreover, parameters numbers have been minimized. ReLU layers which are inserted among undersized convolution layers are really useful.

The input video frame images and their corresponding map video frame images are S = (S (1) … S (N)) and M = (M (1) … M (N)) respectively. The major objective is to design a model which maps StoM with the help of some training data. This is modeled as a probabilistic approach by learning the model of distribution over labels which is represented as shown Eq. (9) and Eq. (10):

$$P\big(n(M,i,w_m)\big|n(S,i,w_s)\big) \tag{9}$$

where, n (I, i, w) is a patch with w*w size for image I, focused on pixel i. Here, w_s is preferred to be higher so that more contextual information can be extracted. Its functional form f is given as:

$$f_i(s) = \sigma\big(a_i(s)\big) = P(m_i = 1|s) \tag{10}$$

where, a_i and f_i represents the sum of input for the ith output and significance of ith output component respectively. σ (x), a logistic utility, is expressed as shown in Eq. (11):

$$\sigma(x) = \frac{1}{1+exp\ (-x)} \tag{11}$$

ALEXNET CNN alongside softmax output unit is used for multi-class marking. The softmax output is a vector of size L which demonstrates the conveyance more than potential marks for pixel i. along these lines for multi-class marking, if path from pixel i to output unit l is thought of, the re-composed condition is:

$$f_{il}(s) = \frac{exp\ (a_{il}(S)}{z} = P(m_i = l|s) \tag{12}$$

Shown Eq. (12) where $f_{il}(s)$ is the prediction probability where pixel I is mapped to label j. The advantages of the proposed method are summarized as below:

First, ALEXNET CNN possibly handles huge amount of labelled data from various domains.

Secondly, it is faster when paralleled with Graphics Processing Unit (GPU). Hence this is also extended for a greater number of pixels. For training data that is simulated by minimizing kernels size through computational learning process of proposed method.

Every patch in training data has been given by initiative sigma. Due to the large number of training patches, optimization becomes complicated. This can be done using binary classifier that uses minimum patches [13]. Few of the hyper parameters have been altered to some extent. The analysis over sensitivity has been defined by hyper parameters for them to be tuned with higher accuracy.

5.2 ALEXNET CNN-MLP (Multilayer Perceptron) based feature extraction

A Rectified Linear Unit (ReLU) is employed as the purpose for each neuron in the information and mystery levels, however a "right away" art piece is used in the final layer. The records layer of the underlying MLP has eight neurons and treats mathematical/downright facts as a single dimensional cluster. The buried layer is made up of four neurons, while the last layer is made up of a single neuron. Three convolution layers and three pooling layers are also included in the planned ALEXNET CNN version (Max Pooling). The previously hidden layer is a convolutional layer made of sixteen detail maps with a sixty 4-pixel piece length and actuation paintings through "ReLu" [14]. Then there may be the pooling layer, it truly is described as taking the most excessive properly really worth controlled by means of a pool period of (2,2). The next pooling layer, it is observed through the initiation work ReLU, stays a thick layer that grips 16 neurons. A thicker layer with 4 neurons emerges as a end result. Two distinct outcomes obtained from two different model fashions: one from the

MLP model and one from the ALEXNET CNN model. The yields are grouped together and analysed as a single set of data. To account for the newly revealed unmarried information as important statistics, two thick layers, each containing four neurons, were implemented. The Keras beneficial API modified into used to attach the MLP and ALEXNET CNN strategies, because it offers a destiny threat to progress models with a confined wide variety of statistics resources and returns. By and large, such models consolidate contributions from some layers utilizing an additional layer and union a few tensors that display the exhaustive graph of the proposed begin to finish model. To total, the mathematical/downright facts property and the contribution as vector inputs are coded and later linked the ones vectors [15]. Eventually, the yield layer has one neuron for the 2 instructions and an instantaneous enactment functionality to introduce probability-like forecasts for each class.

5.3 Feature fusion

This section introduces the GA-based multi-feature fusion model. Every feature's significance must be differentiated in line with the applications and criteria presented in Figure 4. To achieve dynamic weight jobs, a multi-feature fusion model is suggested. The multi-feature fusion strategy is depicted in Figure 5 as a flow chart. As displayed in Figure 6, weights of every feature are randomly initialized and later devise a splicing vector alongside these features & their weights respectively. Each image has a splicing vector, then these weights are divided by the total images. n weight is entirely in a splicing vector, and the ultimate accuracy will be immense if amalgamated [16]. Crux is then a parameter n optimization problem.

This optimization issue is solved by GA. In entire process of making multi-feature fusion approach chief issue remains to make splicing vector & fitness function. Later, these two points are introduced in detail. Initially, splicing vector is constructed, and structure of the same is shown in Figure 5. Let vin be the i-th picture's n-th feature vector, and wn the weight [17]. The VGG-16 feature vector and, subsequently, the characteristic extraction community vector are crucial in our method, despite the fact that opportunity function vectors are possible due to the want for precision. The weights of nugatory vectors can be zero after education, and they'll haven't any impact at the very last effects.

The goal is to maximise the formula below by obtaining w1, w2, ..., wn.

$$\begin{gathered} argmax\left\{f[V_{i=1}^{k}\left(w_1.v_{i1}, w_2.v_{i2}\ldots.., w_n.v_{in}\right]\right\} \\ s.t.w_1 + w_2 + \cdots .+w_n = 1 \\ 0 \le w_1, w_2 \ldots . w_n \le 1 \end{gathered} \tag{13}$$

Here, the outcome of vector vi1 and its weight w1 is w1 vi1. The splicing vector for the i-th photo is Vi (*) and the number of pictures in the positive and negative databases is k. f (V) is the most recently approved precision after splicing feature vectors. The next step is to determine the definite values of w1, w2, ---- wn in order to maximise f. (V). As illustrated in Eq. (13), each of these n weights must fulfil a value between 0 and 1, with a total of 1. The GA fitness function is then calculated. The picture feature's core feature remains that it allows various images to be detectable in a limited number of dimensions. In Figure 6, different color point sets illustrate feature communities of distinct classes. The range of distribution centers among each class regulates the complication in the classification if the statistics of different groups such as variance or dispersion grade are determined. Accuracy of final grouping can be translated into Euclidean vector distance between groups as shown in Figure 7.

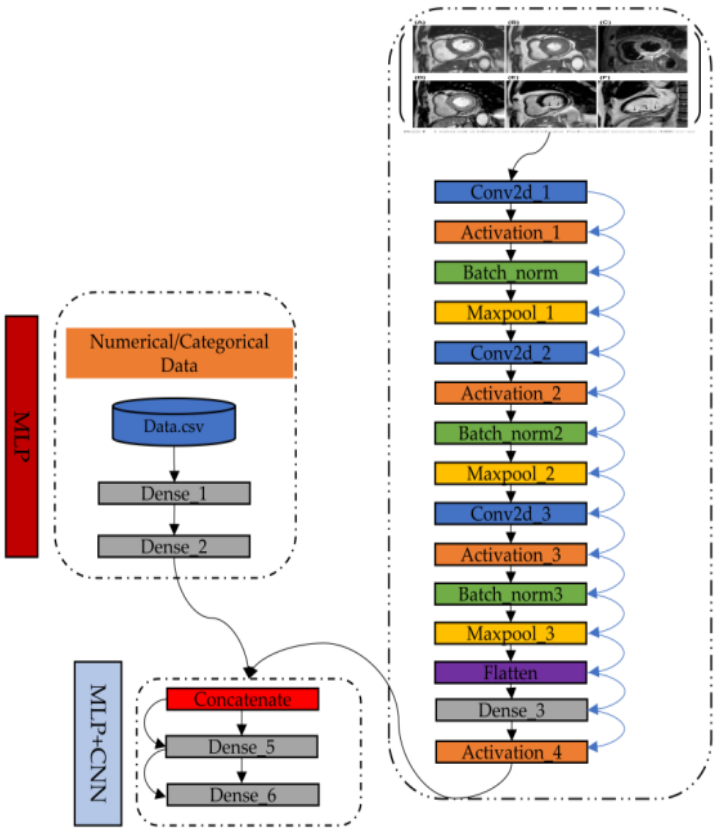

Figure 4. ALEXNET CNN-MLP architecture

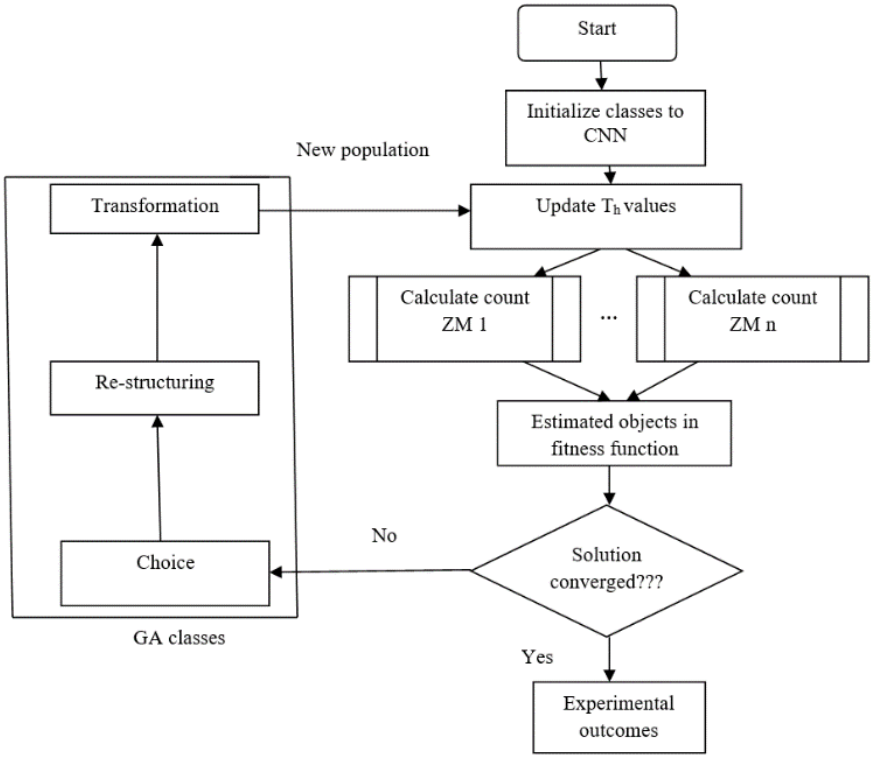

Figure 5. Flowchart of a GA-based multi-feature fusion model

Figure 6. The structure of weighted splicing vector

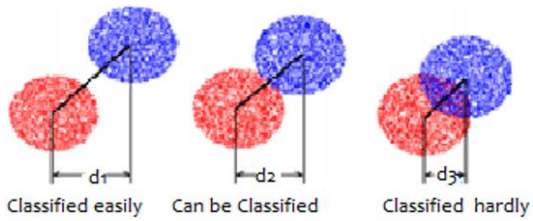

Figure 7. Cluster-based features classification

The common vectors for every elegance are computed, with one common vector and n weight parameters for every elegance. As a result, f($V_{i=1}^{k}$) Eq. (14) could be demonstrated as distance d between two points. If a set of weights w1, w2, ..., wn is found, the optimum inter, splicing vector can be determined. The following is the average inter-class distance:

$$d_{inter} = \sum_{i=1}^{n}\sum_{j=1}^{n} dist(N_i, N_j)/2n \tag{14}$$

where,

$$N_i = \frac{Avg_i}{\sqrt{\sum_{k=1}^{length} Avg_k^2}}, Avg_i = \frac{\sum_{j=1}^{k} V_{ij}}{k} \quad (i = 1,2,3,\ldots,N) \tag{15}$$

where, N suggests the type of training and Avgi denotes the not unusual vector of the i-th elegance. V ij stands for the j-th splicing vector of the i-th elegance. In Eq. (15), dist(Ni,Nj) is the distance among Ni and Nj, and Ni is the normalised vector of Avg. The distances among each Ni I = 1, 2, ..., N) are calculated, and the commonplace charge of these distances is in the long run obtained. The maximum charge of coronary heart valve distances may be converted from the most steeply-priced post-schooling class accuracy.

Hence, the classification precision function is transformed into the splicing vector's function. Amount of weights in splicing vectors probably is enormous. Taking into account the precision of every weight, it is difficult to do the direct calculation. The core of GA is group search that detects optimum solution as per fittest generational evolution's survival principle. Thus, GA is applied towards calculate proper values of w1, w2, ..., wn. As the standards from w1 towards wn are present, arg max(dinter) in Eq. (16) can be effortlessly solved. Thus, fitness function is defined as below.

$$fit(x)d_{inter} = \frac{k}{\sqrt{\sum_{k=1}^{length} Avg_k^2}} \sum_{i=1}^{n}\sum_{j=1}^{n} dist\left(\sum_{a=1}^{k} V_{ia}, \sum_{a=1}^{k} V_{ja}\right) \tag{16}$$

Previously, x was made up of n weights, and every V is made up of n weights as well. Finally, in the feature of fusion method, the remaining aspects of GA are introduced. Initialization, selection, crossover, mutation, and global convergence are the five steps of GA. A few parameters are determined at the startup step: crossover probability, evolutionary generation, group size, mutation probability, and termination stage. Generally, enormous crossover probability & mutation probability could speed up the fitness curve's convergence alongside oscillation following convergence.

The 1000 binary integer, composed of 10 numbers, is 1111101000. Thus, ten digits selected at random between 0 and 1 can be formulated. Many of these codes are composed of a 1 row and n to 10 columns vector. This vector can be

divided into nights as a single entity. Then each person's fitness value is determined using the equation fitness function (7). Fitness results ensure each person's longevity. Roulette collection is used to ensure that those with a huge health appeal will live with huge possibilities. In order to achieve an optimum global solution, elitist filtering is used to keep the best person of any age [18]. Two easy stages are crossover and mutation. Multi-point crossover is used in our approach. Any of their vector elements are transferred to the same location by two people. One digit is at some stage reversed in mutation. The odds of crossover and mutation during initialization are constantly stable.

Every generation's breeding process results in the mutation of one person and the crossover of multiple people, possibly resulting in the birth of a new person. Fitness value of every individual is calculated, then some old individuals are eliminated employing the roulette method. Lasting individuals continue reproducing until the convergence of the fitness curve. Later, we will have the fittest individuals and will be able to gain the best weights from w1 to wn. In the wake of applying GA, weights are allocated to each element vector and another combination includes vector is made dependent on these component vectors and their weights.

5.4 Ensemble classifier

For classification and regression, the ALEXNET CNN approach is used. Data points in ALEXNET CNN models are categorized into categories representing space and points with identical characteristics within the same category. The p-dimensional vectors in linear ALEXNET CNN are considered for the data supplied then are separated thru up to p − 1 planes called hyperplanes. These planes are used for grouping and regression purposes to partition the space between different data classes. The following is a mathematical representation of the SVM. Equation of line is outlined as shown in Eq. (17) to Eq. (19).

$$a_1 = a_2 x + b \tag{17}$$

In Eq. (1) 'x' stands for the line's slobe and 'b' stands for intersect,

$$a_1 - a_2 x + b = 0 \tag{18}$$

Let $\mathrm{a}' = (\mathrm{a}_1, \mathrm{a}_2)^{\mathrm{T}}$ and $\mathrm{z}' = (\mathrm{x}, -1)$ Thus, the above equation can be written as

$$z'.a' += 0 \tag{19}$$

Two-dimensional vectors are used to derive Eq. (20) and Eq. (21). The equation above holds true for any number of dimensions. The hyper lane equation (Eq. (22) and Eq. (23)) remains another name for it. Vector direction $\mathrm{a}' = (\mathrm{a}_1, \mathrm{a}_2)^{\mathrm{T}}$ is mentioned in the form of z' and explained as Eq. (24) to Eq. (26).

$$z' = \frac{a_1}{\| a \|} + \frac{a_2}{\| a \|} \tag{20}$$

where,

$$\| a \| = \sqrt{a_1^2 + a_2^2 + a_3^2 + \cdots . a_n^2} \tag{21}$$

As we know that

$$cos(\theta_1) = \frac{a_1}{\| a \|} \; and \; cos(\theta_2) = \frac{a_2}{\| a \|} \tag{22}$$

Thus, Eq. (3) could also be composed

$$z' = (cos(\theta_1), cos(\theta_2)) \tag{23}$$

$$z'.a = \| z \| \| a \| cos(\theta) \tag{24}$$

$$\begin{gathered} \theta = \theta_1 - \theta_2 \\ cos(\theta) = \cos(\theta_1 - \theta_2) \\ = cos(\theta_1) cos(\theta_2) + sin(\theta_1) sin(\theta_2) \\ = \frac{z'_1}{\| z' \|} \frac{a_1}{\| a \|} + \frac{z'_2}{\| z' \|} \frac{a_2}{\| a \|} \end{gathered} \tag{25}$$

$$\frac{z'_1 a_1 + z'_2 a_2}{\| z' \| \| a \|}, z'.a' = \sum_{i=1}^{n} z'_i a_i \tag{26}$$

The dot end result of a pinnacle circumstance is calculated as f = y(z a + b) for n-dimensional vectors, with signal (f) > 0 denoting accurate categorization and sign (f) 0 denoting erroneous categorization. F is calculated on a education dataset if D is the required dataset shown in Eq. (27) and Eq. (28).

$$f_i = y_i(z'.a + b) \tag{27}$$

The following is how we compute a dataset's functional margin (F):

$$F = min_{i=1 \ldots m} f_i \tag{28}$$

The hyperplane with the largest F will be picked base on the contrast between hyperplanes, with F referring to the geometric mean of the dataset shown in Eq. (29) and Eq. (30). The ideal z and b values for choosing the best hyperplane should be identified. The Lagrangian function is found below Eq. (31) to Eq. (33).

$$L(z', b, \alpha) = \frac{1}{2} z'.z' - \sum_{i=1}^{m} \alpha_i [y: (z'.a + b) - 1] \tag{29}$$

$$\nabla_b L(z', b, \alpha) = -\sum_{i=1}^{m} \alpha_i y_i = 0 \tag{30}$$

By using Eq. (5) and Eq. (6),

$$z' = \sum_{i=1}^{m} \alpha_i y_i a_i \; and \; \sum_{i=1}^{m} \alpha_i y_i = 0 \tag{31}$$

After replacement of Lagrangian function L we get

$$z'(\alpha, b) = \sum_{i=1}^{m} \alpha_i - \frac{1}{2} \sum_{i=1}^{m} \sum_{j=1}^{m} \alpha_i \alpha_j y_i y_j a_i a_j \tag{32}$$

Thus,

$$max_\alpha \sum_{i=1}^{m} \alpha_i - \frac{1}{2} \sum_{i=1}^{m} \sum_{j=1}^{m} \alpha_i \alpha_j y_i y_j a_i a_j \tag{33}$$

In the event that the reality is over the hyperplane, it is delegated +1 elegance imply HD located, and on the off threat that it is beneath the hyperplane, it's miles referred to as 1 magnificence imply HD not decided.

5.5 ADA boost

The ADA boost technology is continually taking decisions from weight balancing process. So that classification becomes simpler through this Machine learning method.

{h(x, ∈ k) k=1, 2, ….}
in which,
{Θk} → identically dispersed independent random vectors.

At input x, the most favored class is cast a unit vote by each tree. Breiman followed below steps, to produce a single tree in ADA Boost.

(1) From the earliest data, at random sample N cases with replacement, where N is # cases in the training set. The growing tree'll have new cases as training set.

(2) At each node out of the M, at random m variables are selected (where, M → input variables and m << M). The node is separated at which these m variables are separated at best. During growth of the forest, m is kept as constant.

(3) Without pruning, each tree attains its full growth.

In the forest, collective trees are brought into through this method; The Ntree parameter decides # trees in advance. The variable m is also named as mtry or k literally. # instances in the leaf node (aka parameter node size) controls the tree's depth and its default value is 1. Aiming to classify a new instance, the above steps are followed to the train/built the forest and once it's done, each grown tree in the forest, undergoes the same run [19]. Votes are recorded for every classification done by each tree on the new instance. The new instance is classified as the class, which gets the maximum votes taking account of all tress. For a provided input variable, every tree possesses the right to vote to choose the finest classification outcome. The specific process is exhibited in Figure 8.

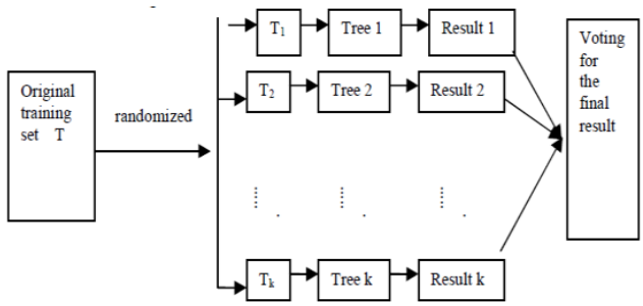

Figure 8. ADA boost classification

We refer Forest RI generated decision tress as Random Forest, here on. Initial instances of about one-third are left out for each tree, when an active sample set is taken out by sampling with replacement. These instances are termed as Out-of-bag (OOB) data. In the forest, each tree's error is estimated from its own OOB data set and named as OOB error estimation. In Random forest, the following are:

(1) PE * = P x,y (mg(X,Y)) < 0 → Generalized error

(2) mg (X,Y) = avk I(hk (X) = Y) – max j≠Yavk I(hk (X) = j)→ refers to margin function

(3) The margin function is a measure of how much the average # of votes for the appropriate class at (X, Y) exceeds the average vote for any other class.

(4) S = E X, Y (mg (X, Y)) → Strength of Random Forest

(5) PE* ≤ ρ (1 – s 2) / s2 → Upper bound of Generalized error where, $\underline{\rho}$ → mean value of correlation b/w base trees.

Thus, it implies accuracy of ADA Boost. is in direct relationship with diversity and accuracy of the base decision trees.

The Table 1 and Figure 8 analysis the comparison of proposed fusion based Deep learning architecture empowered with Ensemble classifier merged with presently available methods is explained, and it has been analyzed with the various existing Deep learning algorithms. The below comparison table clearly giving information about past models and also shown in Figure 8.

6. DATASET DESCRIPTION

Two separate heart disease datasets were used to evaluate Cleveland and Hungarian's proposed model. These datasets are from the online ML and data mining library at the University of California, Irvine (UCI) [14]. These sets of data are employed to classify patients with the cardiac disease that is achieved by assigning a number to each patient: 1 (present) or 0 (absent) (absent). There are 303 cases in the Cleveland dataset, each with 76 features. Just 14 and 16 characteristics were analyzed in our study to determine the health status of a patient. There are 294 cases in the Hungarian dataset, each with 14 attributes. Missing values occur in both datasets, which are addressed by the suggested filtering method described in Dimensionality reduction techniques to remove the dataset's null values [20]. For a more detailed examination of the proposed process, we merged these sets of data to create a single dataset. There are 597 cases in total with 14 attributes in the combined dataset. It must be considered that the Hungarian and amalgamated datasets each have fourteen features, while the dataset of Cleveland only has 16 components. For a categorical dataset, a deep learning model cannot be employed. As a result, categorical data were transformed into numeric data prior to the usage of the deep learning model shown in Figure 9.

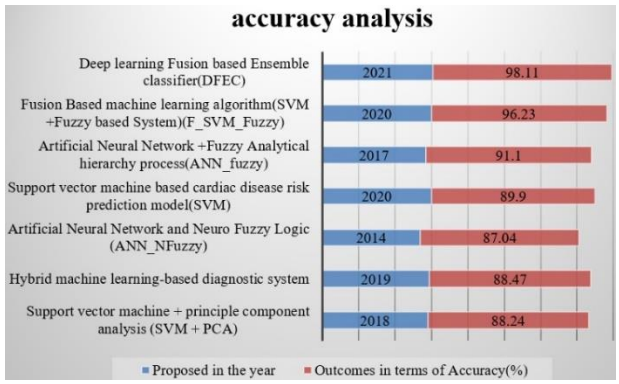

Figure 9. Comparative results

6.1 Performance evaluation

6.1.1 Accuracy

It indicates the actual proportion of categorised cases in the categorization process. It is established as follows:

$$\text{Accuracyrate} = \frac{\text{TruePositive} + \text{TrueNegative}}{\text{TotalInstances}} * 100$$

6.1.2 Precision

This measure is depicted as the true positives' numbers separated by the true positives plus number along with the false positives' numbers. This is used to assess the accuracy and quality of heart disease data, as demonstrated below:

$$\text{Precision} = \frac{\text{Truepositive}}{\text{Truepositive} + \text{FalsePositive}}$$

Table 2 affords a few information of training observations, and the classifier's final results has been expected the usage of the statistics of education. Sets datasets instances, then classifies the times the use of the identical statement, then compares the performance of diverse methods such as SVM+PCA, ANN Nfuzzy, and F SVM+fuzzy to the cautioned DFEC techniques. Performance in Accuracy, AUC, F1-score, Precision, and Recall are compared in Table 2. It was calculated using the actual and expected values from the classes of the aim of confusion matrix, and it is expressed as a percentage [21].

Table 1. Comparative evaluation of proposed architecture with presently available methods in terms of accuracy

Journal	Techniques	Proposed in the year	Outcomes in terms of Accuracy (%)
[11]	Support vector Deep + principle component analysis (SVM + PCA)	2018	88.24
[14]	Hybrid Deep learning-based diagnostic system	2019	88.47
[17]	Artificial Neural Network and Neuro RRS segmentation (ANN_NFuzzy)	2014	87.04
[18]	Support vector Deep based cardiac disease risk prediction model (SVM)	2020	89.9
[10]	Artificial Neural Network +Fuzzy Analytical hierarchy process (ANN_fuzzy)	2017	91.1
[12]	Fusion Based Deep learning algorithm (SVM +Fuzzy based System) (F_SVM_Fuzzy)	2020	96.23
Proposed architecture	Deep learning Fusion based Ensemble classifier (DFEC)	2021	98.11

Table 2. Analysis of performance comparative of proposed architecture alongside existing methods

S.NO	Techniques	SVM+PCA	ANN_fuzzy	F_SVM+fuzzy based	Proposed DCALEXNET CNN_ALEXNET CNNMLP (fusion)
1	Accuracy	88.24	87.04	96.23	98.29
2	Precision	87.11	86.8	95.11	97.21
3	Recall	86.27	84.11	93.21	96.12
4	F1-score	85.17	83.18	92.11	95.56
5	AUC	84.21	82.15	91.23	98.32

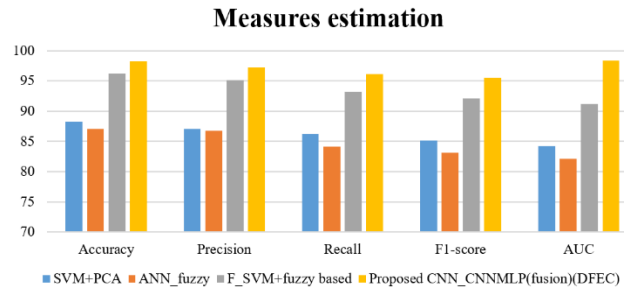

Figure 10. Performance measure estimation

Figures 10 and 11 depicts the disparity between different approaches in terms of accuracy. It is a comparison of existing and planned strategies in terms of accuracy for clinical dataset S [22]. Proposed DFEC achieves Accuracy through a maximum percentage than existing approaches, as indicated in the graph above. Whereas, SVM+PCA, ANN_Nfuzzy, F_SVM+fuzzy method has ensued in the lamest Performance by providing a least of the value of Accuracy of about 88.24%, 87.04%, 96.23%. Finally, the Proposed_DFEC approach executes more proficiently comparing with alternative prototypes by obtaining the highest accuracy value of 98.11%.

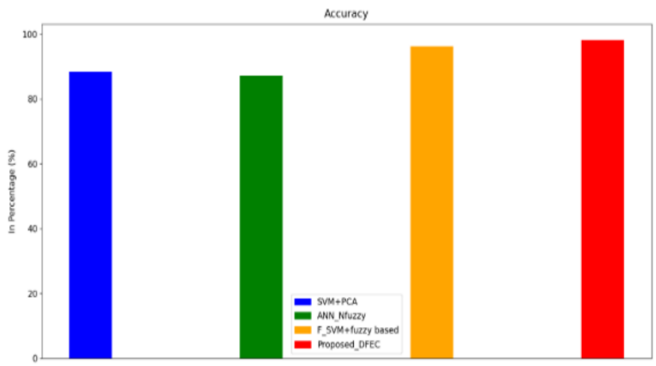

Figure 11. Accuracy comparison of various existing techniques with Proposed_DFEC by applying heart disease _UCI dataset

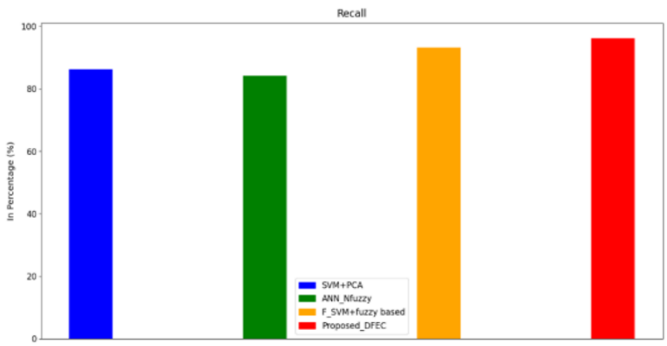

Figure 12. Recall comparison of various existing techniques with Proposed_DFEC by applying heart disease _UCI dataset

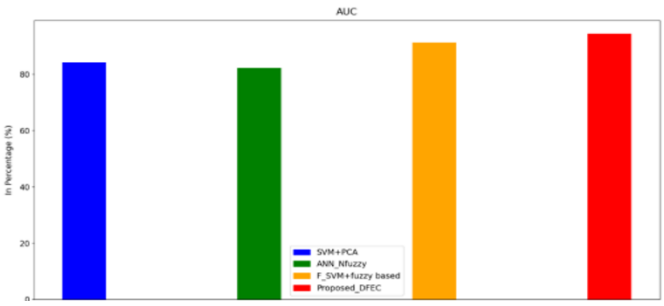

Figure 13. AUC comparison of various existing techniques with Proposed_DFEC by applying heart disease _UCI dataset

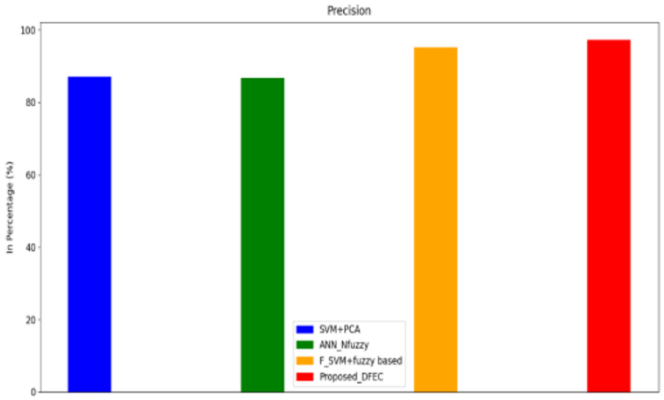

Figure 14. Precision comparison of various existing techniques with Proposed_DFEC by applying heart disease _UCI dataset

The discrepancy between different approaches in terms of recollection is illustrated in Figure 12. It's a comparison of existing and planned approaches for clinical datasets in terms of recall [23]. As demonstrated in the graph, the Proposed DFEC outperforms existing approaches in terms of Recall by a large margin. Whereas, SVM+PCA, ANN_N fuzzy technique has ensued in the lamest peADA Boost. rmance by providing the least value of Precision of about 86.27%, 84.1%. Whereas, F_SVM+fuzzy gradually increase the Recall value of about 93.21% than the other existing techniques. Finally, the proposed Proposed_DFEC approach executes more proficiently comparing with alternative prototypes through obtaining the highest Recall value of 96.12%.

Figure 13 depicts the contrast between different techniques in terms of AUC. It's an AUC comparison of existing and proposed approaches for clinical datasets [24]. As seen in the graph above, the Proposed DFEC obtains a higher AUC than existing approaches by a large margin. Whereas, SVM+PCA, ANN_Nfuzzy technique has ensued in the lamest Performance by providing the least value of Precision of about 84.21%, 82.15%. F SVM+fuzzy, on the other hand, steadily increases the AUC value by roughly 91.23 percent over the other available approaches. Finally, the proposed Proposed_DFEC approach executes more proficiently comparing with alternative prototypes by obtaining the highest AUC value of 94.32%.

Figure 14 depicts the comparison between different approaches in terms of precision. It's a precision comparison of existing and planned approaches for clinical datasets. Proposed DFEC delivers Precision with a maximum percentage than existing approaches, as demonstrated in the above figure. Whereas, SVM+PCA, ANN_Nfuzzy technique has ensued in the lamest peADA Boost. rmance by providing the least value of Precision of about 87.11%, 86.8%. F_SVM+fuzzy on the other hand, steadily increases the AUC value to around 95.11 percent, which is higher than the other available approaches. Finally, the proposed Proposed_DFEC approach executes more proficiently comparing with alternative prototypes by obtaining the highest Precision value of 97.21%.

Figure 15 depicts the contrast between different approaches in terms of F1-score. It's an F1-score comparison of existing and proposed approaches for clinical datasets. As demonstrated in the graph above, the Proposed DFEC produces a higher F1-score than existing approaches by a large margin. Whereas, SVM+PCA, ANN_Nfuzzy technique has ensued in the lamest peADA Boost. rmance by providing the least value of F1-score of about 85.17%, 83.18%. F SVM+fuzzy, on the other hand, gradually increases the F1-score value by roughly 92.11 percent, compared to the other available approaches [25]. Finally, the proposed Proposed_DFEC approach executes more proficiently comparing with alternative prototypes through obtaining the highest F1-score value of 95.56%.

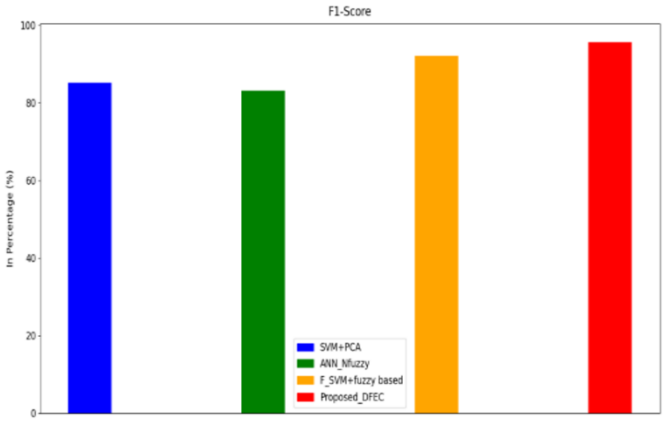

Figure 15. F1-score comparison of various existing techniques with Proposed_DFEC by applying heart disease _UCI dataset

7. CONCLUSION

This research work is concentrated on prior stage heart disease diagnosis in an accurate manner. This prediction mechanism is mainly depending on 13 attributes in the selected dataset (Kaggle). The Genetic algorithm is determining the number of lead alignments in the ultrasound image.csv file that helps the feature extraction processes. In this contest 13 classes are normalized to 6 attributes, nothing but clustering had been done. The images were pre-processed and classified through RRF as well as DCAlexNet CNN techniques. The MLP function is providing feature fusion with text and image datasets. The proposed method is differentiating with AdA boost, GA, SVM+PCA, ANN_fuzzy and F_SVM+fuzzy methodologies. The proposed DCAlexNet CNN MLP method is improved compared to the following models. To this feature fusion performance measures like accuracy 98.67%, sensitivity 97.45%, Recall 99.34% and F1 Score 99.34%, these numerical comparison results compete with present technology and outperformance application robustness.

REFERENCES

[1] Tharwat, A., Gaber, T., Awad, Y.M., Dey, N., Hassanien, A.E. (2016). Plants identification using feature fusion technique and bagging classifier. In the 1st International Conference on Advanced Intelligent System and Informatics (AISI2015), Beni Suef, Egypt, pp. 461-471. https://doi.org/10.1007/978-3-319-26690-9_41

[2] Duarte, D., Nex, F., Kerle, N., Vosselman, G. (2018). Multi-resolution feature fusion for image classification of building damages with convolutional neural networks. Remote Sensing, 10(10): 1636. https://doi.org/10.3390/rs10101636

[3] Mangai, U.G., Samanta, S., Das, S., Chowdhury, P.R. (2010). A survey of decision fusion and feature fusion strategies for pattern classification. IETE Technical Review, 27(4): 293-307.

[4] Zhang, C., Chen, Y., Yang, X., et al. (2020). Improved remote sensing image classification based on multi-scale feature fusion. Remote Sensing, 12(2): 213. https://doi.org/10.3390/rs12020213

[5] Imani, M., Ghassemian, H. (2020). An overview on spectral and spatial information fusion for hyperspectral image classification: Current trends and challenges. Information Fusion, 59: 59-83. https://doi.org/10.1016/j.inffus.2020.01.007

[6] Hasan, R.I., Yusuf, S.M., Alzubaidi, L. (2020). Review of the state of the art of deep learning for plant diseases: a broad analysis and discussion. Plants, 9(10): 1302. https://doi.org/10.3390/plants9101302

[7] Hassan, M.R., Huda, S., Hassan, M.M., Abawajy, J., Alsanad, A., Fortino, G. (2022). Early detection of cardiovascular autonomic neuropathy: A multi-class classification model based on feature selection and deep learning feature fusion. Information Fusion, 77: 70-80.

[8] Abadpour, A., Kasaei, S. (2005). Pixel-based skin detection for pornography filtering. Iranian Journal of Electrical and Electronic Engineering, 1(3): 21-41. https://doi.org/10.1016/j.inffus.2021.07.010

[9] Khan, R.U., Alkhalifah, A. (2018). Media content access: Image-based filtering. International Journal of Advanced Computer Science and Applications, 9(3): 415-419.

[10] Murat, F., Yildirim, O., Talo, M., Baloglu, U.B., Demir, Y., Acharya, U.R. (2020). Application of deep learning techniques for heartbeats detection using ECG signals-analysis and review. Computers in Biology and Medicine, 120: 103726. https://doi.org/10.1016/j.compbiomed.2020.103726

[11] Huang, C., Lan, Y., Xu, G., et al. (2020). A deep segmentation network of multi-scale feature fusion based on attention mechanism for IVOCT lumen contour. IEEE/ACM Transactions on Computational Biology and Bioinformatics, 18(1): 62-69. https://doi.org/10.1109/TCBB.2020.2973971

[12] Iqbal, N., Hanif, M. (2021). An efficient grayscale image encryption scheme based on variable length row-column swapping operations. Multimedia Tools and Applications, 80(30): 36305-36339. https://doi.org/10.1007/s11042-021-11386-x

[13] Wang, H., Zhang, B., Chen, W. (2021). Robust and real-time object recognition based on multiple fractal dimension. Multimedia Tools and Applications, 80: 36585-36603. https://doi.org/10.1007/s11042-021-11447-1

[14] Dhingra, G., Kumar, V., Joshi, H.D. (2021). Clustering-based shadow detection from images with texture and color analysis. Multimedia Tools and Applications, 80(25): 33763-33778. https://doi.org/10.1007/s11042-021-11427-5

[15] Li, J., Chen, H., Li, Y., Peng, Y., Cai, N., Cao, X. (2021). AMRSegNet: Adaptive modality recalibration network for lung tumor segmentation on multi-modal MR images. Multimedia Tools and Applications, 80(25): 33779-33797. https://doi.org/10.1007/s11042-021-11225-z

[16] Dong, B., Wang, R., Yang, J., Xue, L. (2021). Multi-scale feature self-enhancement network for few-shot learning. Multimedia Tools and Applications, 80(25): 33865-33883. https://doi.org/10.1007/s11042-021-11205-3

[17] Almaraz-Damian, J.A., Ponomaryov, V., Sadovnychiy, S., Castillejos-Fernandez, H. (2020). Melanoma and nevus skin lesion classification using handcraft and deep learning feature fusion via mutual information measures. Entropy, 22(4): 484. https://doi.org/10.3390/e22040484

[18] Wang, C., Elazab, A., Wu, J., Hu, Q. (2017). Lung nodule classification using deep feature fusion in chest radiography. Computerized Medical Imaging and Graphics, 57: 10-18. https://doi.org/10.1016/j.compmedimag.2016.11.004

[19] Chandra, M.A., Bedi, S.S. (2021). Survey on SVM and their application in image classification. International Journal of Information Technology, 13(5): 1-11. https://doi.org/10.1007/s41870-017-0080-1

[20] Ramaiah, V.S., Singh, B., Raju, A.R., Reddy, G.N., Saikumar, K., Ratnayake, D. (2021). Teaching and learning based 5G cognitive radio application for future application. In 2021 International Conference on Computational Intelligence and Knowledge Economy (ICCIKE), Dubai, United Arab Emirates, pp. 31-36. https://doi.org/10.1109/ICCIKE51210.2021.9410797

[21] Mohammad, M.N., Kumari, C.U., Murthy, A.S.D., Jagan, B.O.L., Saikumar, K. (2021). Implementation of online and offline product selection system using FCNN deep learning: Product analysis. Materials Today: Proceedings, 45: 2171-2178. https://doi.org/10.1016/j.matpr.2020.10.072

[22] Padmini, G.R., Rajesh, O., Raghu, K., Sree, N.M., Apurva, C. (2021). Design and analysis of 8-bit ripple carry adder using nine transistor full adder. In 2021 7th International Conference on Advanced Computing and Communication Systems (ICACCS), Coimbatore, India, pp. 1982-1987. https://doi.org/10.1109/ICACCS51430.2021.9441928

[23] Saba, S.S., Sreelakshmi, D., Kumar, P.S., Kumar, K.S., Saba, S.R. (2020). Logistic regression machine learning algorithm on MRI brain image for fast and accurate diagnosis. International Journal of Scientific and Technology Research, 9(3): 7076-7081.

[24] Saikumar, K., Rajesh, V. (2020). Coronary blockage of artery for heart diagnosis with dt artificial intelligence algorithm. International Journal of Research in Pharmaceutical Sciences, 11(1): 471-479.

[25] Sreelakshmi, D., Inthiyaz, S. (2021). Fast and denoise feature extraction based ADMF–CNN with GBML framework for MRI brain image. International Journal of Speech Technology, 24(2): 529-544. https://doi.org/10.1007/s10772-020-09793-w